Journal Pre-proof


# Surface acoustic wave ammonia sensor based on ZnS mucosal-like nanostructures

Gongdi Long, Yuanjun Guo, Wei Li, Qingbo Tang, Xiaotao Zu, Jinyi Ma, Bo Du, Yongqing Fu

PII: S0167-9317(19)30357-0

DOI: https://doi.org/10.1016/j.mee.2019.111201

Reference: MEE 111201

To appear in: *Microelectronic Engineering*

Received date: 12 August 2019

Revised date: 9 December 2019

Accepted date: 18 December 2019

Please cite this article as: G. Long, Y. Guo, W. Li, et al., Surface acoustic wave ammonia sensor based on ZnS mucosal-like nanostructures, *Microelectronic Engineering* (2019), https://doi.org/10.1016/j.mee.2019.111201

# Surface acoustic wave ammonia sensor based on ZnS mucosal-like nanostructures

Gongdi Long[1,#], Yuanjun Guo[1,*], Wei Li[2,#,*], Qingbo Tang[1], Xiaotao Zu[1], Jinyi Ma[3], Bo Du[3] and Yongqing Fu[4,*]

[1] School of Physics, University of Electronic Science and Technology of China, Chengdu, 610054, People's Republic of China

[2]School of Chemistry, Physics and Mechanical Engineering, Queensland University of Technology, Brisbane, Queensland 4001, Australia

[3] Sichuan Institute of Piezoelectric and Acousto-Optic Technology, Chongqing 400060, People's Republic of China

[4] Faculty of Engineering & Environment, University of Northumbria, Newcastle upon Tyne, NE18ST, UK



# These authors contributed equally to this work

*Corresponding authors.

E-mail address:

guoyuanjun@uestc.edu.cn,

w74.li@qut.edu.au,

and Richard.fu@northumbria.ac.uk

**Abstract:** Mucosal-like ZnS nanostructures were synthesized on surface of ST-cut quartz surface acoustic wave (SAW) device using a chemical bath deposition method for ammonia sensing applications. Results showed the SAW device with ZnS mucosal nanostructures achieved a good sensitivity, e.g., with a frequency shift of ~190 Hz upon exposure to 1 ppm ammonia gas. This is mainly attributed to the large specific surface areas and more active sites on the surfaces of the ZnS mucosal nanostructures. Selectivity of the SAW device with the ZnS mucosal nanostructure for ammonia sensing was excellent in comparisons with those for other types of gases such as hydrogen sulfide, hydrogen, nitrogen dioxide, carbon monoxide and ethanol.

**Keywords**: mucosa, ZnS nanostructure, Surface acoustic wave, gas sensor

## 1. Introduction

Ammonia sensing and monitoring are of great importance in environmental gas analysis, automotive industry, chemical industry, and medical applications [1], and high-performance ammonia sensors with high sensitivity, good selectivity and reliability, as well as high precision are critically required. Surface acoustic wave (SAW) technology is considered to be one of the effective methods to prepare high performance gas sensors due to their fast response speed, high sensitivity, good stability and ease of subsequent processing. Many researchers have used SAW technology to prepare different types of gas sensors and achieved good sensing results [2-8]. The principle of the SAW based gas sensing is that the sensitive layer on the SAW device adsorbs the target gas molecules, which causes the changes of mass, conductivity and/or viscoelasticity of the sensitive film, thereby changing the frequency of the SAW device [9-11].

Metal oxides are the most commonly investigated materials for the SAW sensing layer [12]. Various metal oxide semiconductors such as ZnO [5, 7, 8, 13, 14], $SnO_2$ [15-17], $WO_3$ [18-20], $TiO_2$ [3, 21-23], CuO [24-26] have been successfully applied as the gas sensing layers on the SAW devices. Metal sulfides are rarely reported being used in gas sensors compared to those widely reported metal oxides. However, as reported in ref. [27-30], sulfides often show good selectivities for the specifically targeted gases. ZnS has a similar crystal structure with ZnO, with a wide band gap

(3.72 eV) and abundant sulfur vacancies on its surface. Xu et al investigated gas adsorption and electronic properties of ZnS using first-principle calculations, and showed that ZnS is a promising candidate for high-performance sensing applications, especially for $NH_3$ [31]. In recent years, different types of ZnS nanostructures such as nanorods [32], nanowires [33], nanobelts [34], nanoribbons[35], nanotubes [36], and hollow spheres [37, 38] have been widely used in various fields. These nanostructures have larger specific surface areas and more active sites than the dense ZnS film, and thus can be applied to various applications such as in catalysts, photo-detection and gas sensing, which require gas sensors having high sensitivity and good selectivity.

Recently researchers have been inspired by many biological structures in nature and have produced similar structures for specific applications, which is often called bionic design methodology [39-45]. For example, Jian et al. prepared a flexible piezoelectric sensor based on bionic structure with high sensitivity, low detection limit, fast response time and stable performance [43]. Translucent snake-like bionic sensor system prepared by Cai et al. can not only be used to monitor tensile strains, but also achieve a high sensitivity to odorless $CH_4$ gas [45].

As is well known, small intestinal mucosa has an extremely large surface area. For example, our human being's small intestine is about 5 meters long, but has a surface areas of nearly 300 square meters. The reason is that intestinal mucosa has a great number of folds, which make itself much efficient in fast absorption of food. Therefore, if such types of sensing layers with an intestinal mucosa-like structure can

be made on the SAW sensor, the absorption and sensing of the target gas should be much easier and faster. Therefore, we believe that the ZnS based mucosal structures would be a good sensing layer for the SAW gas sensor.

In this paper, mucosa-like ZnS nanostructures were fabricated on the surface of a ST-cut quartz SAW device using a chemical bath deposition method, and their sensitivity and selectivity to ammonia gas were systematically investigated.

## 2. Experimental Details

### 2.1. SAW device and sensing layer preparation

SAW devices were fabricated on ST-cut quartz (42°75′) using the conventional photolithography and metallization processes. Aluminum layer of 200 nm thick was sputtered onto ST-cut quartz substrate and then interdigital transducers (IDTs) were prepared using a lift-off process. The SAW devices had 30 pairs of IDTs and 100 pairs of reflectors. The width of each finger was 4 μm, and the width of the reflectors finger was also 4 μm. The aperture of the IDTs was 3 mm. The resonant frequency of SAW devices was designed to be ~200 MHz.

Chemical bath deposition method [46-48] was used to fabricate the ZnS nanostructures. In order to make the aqueous solution of the ZnS, a mixture was made using 0.045 M zinc acetate dihydrate ($Zn(CH_3COO)_2 \cdot 2H_2O$), 0.065 M thiourea ($H_2NCSNH_2$), 0.133 M tartaric acid ($COOH(CHOH)_2COOH$) and 80% hydrazine hydrate [46]. Firstly, 10 ml zinc acetate solution and 10 ml tartaric acid solution were mixed and stirred for 5 minutes. Then 10 ml thiourea solution was added inside the

above solution and continuously stirred for another 3 minutes to obtain a clear and homogeneous solution. Thereafter, 5 ml of 80% hydrazine hydrate was added into the above solution and stirred for 3 minutes. Finally, ammonia water (25 wt%) was added drop-by-drop into this solution to adjust the pH value of the solution to be ~10.

An ST-cut quartz SAW device was attached onto a glass slide with its IDTs and reflectors fully protected with a polyimide tape. It was then placed inside the ZnS growth solution inside a water bath at a fixed temperature of 85 °C for 30 min. The illustration of the preparation set-up is shown in Figure 1. After a layer of film was deposited onto the device's sensing area between the two opposite IDTs, the quartz SAW device was taken out and then immersed into ethanol for several minutes. It was then ultrasonically cleaned with de-ionized water to remove any residues on the device surface. In order to optimize the ZnS nanostructure, six different ZnS nanostructured samples were prepared onto the quartz SAW devices. The preparation parameters were same, but the growth time was different, e.g., 5, 10, 20, 30, 35 and 40 minutes, respectively. The corresponding samples were named as sample 1, sample 2, sample 3, sample 4, sample 5 and sample 6, respectively.

2.2. Characterization and ammonia sensing techniques

Surface morphologies of ZnS nanostructures were observed using a field-emission scanning electron microscope (FE-SEM, Carl Zeiss 1530 VP, USA). Crystallinity of the prepared ZnS nanostructures was characterized using an X-ray diffractometer (XRD, Rigaku D/max-2400, Japan), with a Cu Kα radiation source and

a wavelength of 0.15406 nm. The scanning rate of the XRD tests was 4 $^{o}$/min and the step length was 0.02$^{o}$.

Figure 2(a) shows a structural illustration of SAW sensor and its corresponding electronic components. The SAW sensor is based on an oscillator which consists of a sensing film coated SAW resonator with its corresponding amplification and phase-shift circuits. Figure 2(b) shows the gas sensing set-up using the SAW ammonia sensor, which includes a SAW resonator coated with the ZnS nanostructures and the corresponding oscillator circuits. The frequency responses of the sensors were recorded using a frequency counter (Agilent 53210, Keysight Technology). A large plexiglassbox with a volume of 20 L was used as the testing chamber. Standard target gases, such as $NH_3$, $H_2$, $H_2S$, $NO_2$ and $CH_3CH_2OH$ were purchased from the National Institute of Testing Technology, China. All the target gases have a concentration of 2%, which was obtained by diluting with pure $N_2$. During the measurement, different volumes of test gases were injected into the test chamber through a precision syringe pump to obtain different concentrations of the tested gas, All the tests were done in a fume cupboard. The ambient temperature was controlled at 25 °C in an air conditioned environment and the ambient relative humidity (RH) value was controlled to be 45% using both a humidifier and a mass flow controller which controls the flow rate of dry air. A network analyzer (Hewlett-Packard 8714C, USA) was used to detect the center frequency of the quartz SAW resonator coated with ZnS nanostructure before and after the targeted gas was injected. When the response reached an equilibrium condition and the test was finished, the chamber was opened and quickly purged with dry air, and the frequency of the SAW devices was monitored.

## 3. Results and Discussions

Figure 3 shows the XRD results of the ZnS film layer which was deposited for 30 min (sample 4). The morphologies of those film groups that were deposited less

than 30 min are not shown in Figure 3 because those films are too thin to obtain high quality images. The XRD pattern shown in Fig. 3 indicates the characteristic peaks at 2θ=26.91°, 47.56° and 56.29°, which correspond to (100), (110), and (103) diffraction peaks of the wurtzite zinc sulfide crystals (JCPDS card No 36-1450), respectively.

Fig. 4 shows SEM images of ZnS nanostructures on ST-cut quartz substrates prepared with different deposition durations, revealing a dynamic growth process of ZnS nanostructures. After 5 min deposition, a smooth ZnS nanofilm has already formed on the device surface. During the further growth, there are a great number of ball-shaped microstructures formed on the surface of ZnS nanofilm. After 20 min film growth, there are some folds formed on the surface of ZnS nanofilm. With the further increase of deposition time, the mucosal structures can be clearly seen, but the spaces between the folds become much smaller, indicating formation of dense mucosal nanostructures. The thicknesses of samples 2, 3 and 4 are 42, 105 and 210 nm, respectively. The thickness of sample 1 is too thin to be measured clearly using the SEM.

Resonant frequencies and insertion losses values of the six groups of SAW resonators are shown in Figure 5. Generally, with the increase of film thickness, the insertion loss is increased and the center frequency is reduced, which is mainly due to the mass loading effect. For example, the center frequencies of sample 1 and sample 3 are ~199.15 and 198.85 MHz, respectively. According to Figure 5, the insertion losses of sample 1 and sample 2 are -11.92 dB and -15.97 dB, respectively. Whereas for

sample 5, the insertion loss is -31.23 dB, while the center frequency is ~ 198.45 MHz. Considering the amplified ability of the amplifiers in circuits and the detecting limitation of frequency counter, the SAW sensors of sample 5 and sample 6 (whose insertion losses are more than -30 dB) will not be used in the following sensing tests.

Figure 6 shows the responses of the SAW devices exposed to the ammonia gas with a concentration of 20 ppm. We can clearly see from Fig. 6(a) that the longer time the ZnS grows, the more significant response of the SAW sensor to ammonia. Figure 6(b) shows the response and recovery times of these SAW sensors to 20 ppm ammonia. Here, the response time is defined as the time required for the frequency shift to reach 90% of its final value. Similarly, the recovery time is defined as the time required for the frequency shift to return to 10% of its total frequency shift value after the target gas is released. These SAW sensors have short response times (e.g., from 6 s to 45 s) but relatively long recovery times (e.g., from 100 s to 148 s) to 20 ppm ammonia. In addition, the recovery time of the SAW sensor becomes longer as the thickness of ZnS layer is increased, which is mainly because the thicker the sensing layer, the larger the surfaces areas, thus the longer time to release the gas molecules.

The frequency shifts of the SAW devices based on ZnS nanostructures of sample 1 and sample 4 were measured when they were exposed to different concentrations of ammonia gas. The measurement results are shown in Figs. 7(a) and 7(b), respectively. Both these two SAW sensors have a negative frequency response to ammonia. In addition, the SAW sensor of sample 4 is found to be more sensitive to ammonia than

that of sample 1, because the mucosal structures in sample 4 have a larger specific surface area.

The main factors that change the frequency of SAW gas sensors are mass loading, acoustoelectric effect (electrical loading) and elastic loading, which can be expressed using the following equation [17]:

$$\frac{\Delta f}{f_0} = (k_1 + k_2) f_0^2 \rho_s - \frac{k^2}{2}\left(\frac{1}{1+\left(\frac{v_0 c_s}{\sigma_s}\right)^2}\right) + c_e f_0 h\left(\left(\frac{4u}{v_0^2}\right)\times\left(\frac{u+\lambda}{u+2\lambda}\right)\right)$$

(1)

where $k_1 = -8.7 \times 10^{-8}$ m$^2$s kg$^{-1}$ and $k_2 = -3.9 \times 10^{-9}$ m$^2$s kg$^{-1}$ are material constants of the ST- cut quartz substrate; $f_0$ is the center frequency of the SAW device which has not been changed (~200 MHz); $\rho_s$ is the surface density of the layer; $k^2$ (0.11% for quartz) is the electromechanical coupling factor; $v_0$ (3158 m/s for quartz) is the unperturbed wave velocity for the SAW device; and $c_s$ (0.5 pF cm$^{-1}$) is the sum of the dielectric permittivity of the substrate and the environment; $\sigma_s$ is the surface conductivity; $c_e$ is the sensitivity coefficients of elasticity, $h$ is film thickness; $\lambda$ is the bulk modulus of elasticity; and $u$ is the shear modules of elasticity. Effects of mass loading, electrical loading and elastic loading on the sensing response are represented by 1st, 2nd, and 3rd term of equation (1), respectively.

When the ZnS-based SAW gas sensor is exposed to the ammonia atmosphere, the ZnS sensitive layer quickly adsorbs ammonia gas molecules and thus causes the mass loading effect. According to the first part of equation (1), the mass loading will

reduce the frequency of the SAW, thus resulting in a negative frequency shift, and this is consistent with our experimental results.

Generally, the surface of the ZnS film adsorbs oxygen molecules through intermolecular forces. Due to the strong oxidizing properties of oxygen molecules, the sensing layer surface will capture a large amount of electrons, resulting in the formation of a depletion layer on the surface of ZnS. At the same time, the oxygen molecules that capture electrons will become $O^{2-}$ ions [49].

$$O_2(gas) \leftrightarrow O_2(ads) \quad (2)$$

$$O_2(ads) + e^- \leftrightarrow O_2^-(ads) \quad (3)$$

When the ZnS film is exposed to ammonia atmosphere, the active $O^{2-}$ ions react with the ammonia molecules adsorbed on the surface of the film to release electrons, as shown in the following reactions [50]:

$$NH_3(gas) \rightarrow NH_3(ads) \quad (4)$$

$$4NH_3(ads) + 3O_2^- \rightarrow 2N_2 + 6H_2O + 3e^- \quad (5)$$

These will result in a decrease in the depletion layer and an increase in the film conductivity. From the second part of Equation 1 (e.g., electrical loading), the frequency is decreased as the conductivity is increased, which will result in a negative frequency shift, and is also consistent with the results of our experiments.

If the SAW sensor adsorbs ammonia, the viscoelasticity of the membrane changes, causing the changes of its wave velocity and frequency. This is generally called elastic loading effect. However, the adsorption of ammonia will increase the

elastic modulus of the sensing film and produce a positive frequency shift [3, 51, 52]. Therefore, the elastic loading is not the main reason for the negative response of the SAW sensor in this study. In summary, the negative frequency shift of the SAW sensor is mainly caused by the mass loading and the acoustoelectric effect.

The selectivity of the ZnS SAW sensor was further tested and compared with those with different types of gases. Figures 7(c) and 7(d) show the responses of sensors (sample 1 and sample 4) to different targeted gases but with a fixed volume of 100 ppm. These two types of SAW devices have shown good selectivity to ammonia, compared with the other five different testing gases, including CO, $NO_2$, $H_2$, $H_2S$, and $CH_3CH_2OH$.

## 4. Conclusion

In this study, we prepared mucosal structures of ZnS-based SAW sensor based on the bionic design methodology, which can improve the sensitivity of the sensor. The SAW sensor showed negative frequency shifts towards ammonia gas, which was caused by mass loading and the electrical loading. The good performance of these mucosal-like ZnS nanostructures is mainly attributed to their large specific surface areas and more active sites on their surface. The selectivity of the SAW device with the ZnS mucosal nanostructure to ammonia gas was excellent in comparison with sensing results for other gases such as hydrogen sulfide, hydrogen, nitrogen dioxide, carbon monoxide and ethanol.

**Acknowledgment**

This study was supported financially by the Fundamental Research Funds for the Central Universities (A03018023801119). Funding supports from UK Engineering Physics and Science Research Council (EPSRC EP/P018998/1), Newton Mobility Grant (IE161019) through Royal Society and NFSC, and Royal academy of Engineering UK-Research Exchange with China and India are also acknowledged.

**References:**

[1] Timmer B, Olthuis W, Van Den Berg A. Ammonia sensors and their applications—a review, Sensors and Actuators B: Chemical. 107 (2005) 666-77

[2] Bo L, Xiao C, Hualin C, Mohammad MA, Xiangguang T, et al. Surface acoustic wave devices for sensor applications, Journal of Semiconductors. 2 (2016) 1-9

[3] Tang Y, Ao D, Li W, Zu X, Li S, Fu YQ. $NH_3$ sensing property and mechanisms of quartz surface acoustic wave sensors deposited with $SiO_2$, $TiO_2$, and $SiO_2$-$TiO_2$ composite films, Sensors and Actuators B: Chemical. 254 (2018) 1165-1173

[4] Tang Y, Li Z, Ma J, Wang L, Yang J, et al. Highly sensitive surface acoustic wave (SAW) humidity sensors based on sol–gel $SiO_2$ films: Investigations on the sensing property and mechanism, Sensors and Actuators B: Chemical. 215 (2015) 283-291

[5] Tang Y-L, Li Z-J, Ma J-Y, Guo Y-J, Fu Y-Q, Zu X-T. Ammonia gas sensors based on ZnO/$SiO_2$ bi-layer nanofilms on ST-cut quartz surface acoustic wave devices, 201 (2014) 114-121

[6] Tang Y-L, Li Z-J, Ma J-Y, Su H-Q, Guo Y-J, et al. Highly sensitive room-temperature surface acoustic wave (SAW) ammonia sensors based on $Co_3O_4$/$SiO_2$ composite films, Sensors and Actuators B: Chemical. 280 (2014) 127-133

[7] Wang S-Y, Ma J-Y, Li Z-J, Su H, Alkurd N, et al. Surface acoustic wave ammonia sensor based on ZnO/$SiO_2$ composite film, Journal of hazardous materials. 285 (2015) 368-374

[8] Li W, Guo Y, Tang Y, Zu X, Ma J, et al. Room-Temperature Ammonia Sensor Based on ZnO Nanorods Deposited on ST-Cut Quartz Surface Acoustic Wave Devices, Sensors. 17 (2017) 1142-1152

[9] Jakubik WP. Surface acoustic wave-based gas sensors, Thin Solid Films. 520 (2011) 986-993

[10] Liang S, Dai Y, von Helden L, Schwarzkopf J, Wördenweber R. Surface acoustic waves in strain-engineered $K_{0.7}Na_{0.3}NbO_3$ thin films, Appl. Phys. Lett. 113 (2018) 052901

[11] Mujahid A, Dickert FL. SAW and Functional Polymers, Gas Sensing Fundamentals. (2013) 213-245

[12] Afzal A, Iqbal N, Mujahid A, Schirhagl R. Advanced vapor recognition materials for selective and fast responsive surface acoustic wave sensors: A review, Analytica Chimica Acta. 787 (2013) 36-49

[13] Y.Q. Fu, J.K. Luo, N.T. Nguyen, A.J. Walton, A.J. Flewitt, X.T Zu, Y. Li, G. McHale, A. Matthews. E. Iborra H. Du,W.I. Milne. Advances in piezoelectric thin films for acoustic biosensors, acoustofluidics and lab-on-chip applications, Progress in Mater Sci. 89 (2017) 31-91

[14] Raj VB, Nimal A, Parmar Y, Sharma M, Gupta V. Investigations on the origin of mass and elastic loading in the time varying distinct response of ZnO SAW ammonia sensor, Sensors and Actuators B: Chemical. 166 (2012) 576-585

[15] Luo W, Deng J, Fu Q, Zhou D, Hu Y, et al. Nanocrystalline $SnO_2$ film prepared by the aqueous sol–gel method and its application as sensing films of the resistance and SAW $H_2S$ sensor, Sensors and Actuators B: Chemical. 217 (2015) 119-128

[16] Luo W, Fu Q, Zhou D, Deng J, Liu H, Yan G. A surface acoustic wave $H_2S$ gas sensor employing nanocrystalline $SnO_2$ thin film, Sensors and Actuators B: Chemical. 176 (2013) 746-752

[17] Raj VB, Nimal A, Tomar M, Sharma M, Gupta V. Novel scheme to improve $SnO_2$/SAW sensor performance for $NO_2$ gas by detuning the sensor oscillator frequency, Sensors and Actuators B: Chemical. 220 (2015) 154-161

[18] Ippolito S, Ponzoni A, Kalantar-Zadeh K, Wlodarski W, Comini E, et al. Layered

$WO_3$/ZnO/36° $LiTaO_3$ SAW gas sensor sensitive towards ethanol vapour and humidity, Sensors and Actuators B: Chemical. 117 (2006) 442-450

[19] Penza M, Tagliente M, Mirenghi L, Gerardi C, Martucci C, Cassano G. Tungsten trioxide ($WO_3$) sputtered thin films for a $NO_x$ gas sensor, Sensors and Actuators B: Chemical. 50 (1998) 9-18

[20] Penza M, Vasanelli L. SAW $NO_x$ gas sensor using $WO_3$ thin-film sensitive coating, Sensors and Actuators B: Chemical. 41 (1997) 31-36

[21] Jakubik WP. Investigations of Thin Film of Titanium Dioxide ($Tio_2$) in a Surface Acoustic Wave Gas Sensor System, Molecular and Quantum Acoustics. 27 (2006) 133-139

[22] Raj VB, Singh H, Nimal A, Sharma M, Gupta V. Oxide thin films (ZnO, $TeO_2$, $SnO_2$, and $TiO_2$) based surface acoustic wave (SAW) E-nose for the detection of chemical warfare agents, Sensors and Actuators B: Chemical. 178 (2013) 636-647

[23] Yan X, Li D, Hou C, Wang X, Zhou W, et al. Comparison of response towards $NO_2$ and $H_2S$ of PPy and PPy/$TiO_2$ as SAW sensitive films, Sensors and Actuators B: Chemical. 161 (2012) 329-333

[24] DJ Li, XT Zu, DY Ao, QF Tang, YQ Fu, YJ Guo, K Bilawal, MB Faheem, L Li, S Li, YL Tang, High humidity enhanced surface acoustic wave (SAW) $H_2S$ sensors based on sol–gel CuO films, Sensors and Actuators B: Chemical. 294 (2019) 55-61

[25] Bae HY, Choi GM. Electrical and reducing gas sensing properties of ZnO and ZnO–CuO thin films fabricated by spin coating method. Sensors and Actuators B: Chemical. 55 (1999) 47-54

[26] Wang X, Wang W, Li H, Fu C, Ke Y, He S. Development of a $SnO_2$/CuO-coated surface acoustic wave-based $H_2S$ sensor with switch-like response and recovery, Sensors and Actuators B: Chemical. 169 (2012) 10-16

[27] Zhong F, Wu Z, Guo J, Jia D. Ni-Doped ZnS Nanospheres Decorated with Au Nanoparticles for Highly Improved Gas Sensor Performance, Sensors. 18 (2018) 2882

[28] Wang X, Xie Z, Huang H, Liu Z, Chen D, Shen G. Gas sensors, thermistor and photodetector based on ZnS nanowires, Journal of Materials Chemistry. 22 (2012) 6845-6850

[29] Liu X-H, Yin P-F, Kulinich SA, Zhou Y-Z, Mao J, et al. Arrays of Ultrathin CdS

Nanoflakes with High-Energy Surface for Efficient Gas Detection, ACS applied materials & interfaces. 9 (2016) 602-609

[30] Navale S, Mane A, Chougule M, Shinde N, Kim J, Patil V. Highly Selective and Sensitive CdS Thin Film Sensor for Detection of $NO_2$ Gas, RSC Advances. 4 (2014) 44547-44554

[31] Xu YX, Ruishen M, Xiong DX, Sun X, Wang SG, Xiao J, Chen XP, Monolayer ZnS as a Promising Candidate for $NH_3$ Sensor: A First-Principle Study, IEEE SENSORS JOURNAL. 20 (2017) 6515-6521

[32] Chen X, Xu H, Xu N, Zhao F, Lin W, et al. Kinetically controlled synthesis of wurtzite ZnS nanorods through mild thermolysis of a covalent organic-inorganic network, Inorganic chemistry. 42 (2003) 3100-3106

[33] Moore DF, Ding Y, Wang ZL. Crystal Orientation Ordered ZnS Nanowire Bundles, Journal of the American Chemical Society. 126 (2004) 14372-14373

[34] Fang X, Bando Y, Liao M, Gautam UK, Zhi C, et al. Single - Crystalline ZnS Nanobelts as Ultraviolet - Light Sensors, Advanced Materials. 21 (2009) 2034-2039

[35] Fan X, Meng XM, Zhang XH, Shi WS, Zhang WJ, et al. Dart-shaped tricrystal ZnS nanoribbons, Angewandte Chemie. 118 (2006) 2630-2633

[36] Huang X, Wang M, Willinger M-G, Shao L, Su DS, Meng X-M. Assembly of three-dimensional hetero-epitaxial ZnO/ZnS core/shell nanorod and single crystalline hollow ZnS nanotube arrays, ACS nano. 6 (2012) 7333-7339

[37] Luo M, Liu J, Hu J, Li J, Liu J, Richards RM. General strategy for one-pot synthesis of metal sulfide hollow spheres with enhanced photocatalytic activity, Applied Catalysis B: Environmental. 125 (2012) 180-188

[38] Zhang L, Dong R, Zhu Z, Wang S. Au nanoparticles decorated ZnS hollow spheres for highly improved gas sensor performances, Sensors and Actuators B: Chemical. 245 (2017) 112-121

[39] Xue C, Chen S, Zhang W, Zhang B, Zhang G, Qiao H. Design, fabrication, and preliminary characterization of a novel MEMS bionic vector hydrophone, Microelectronics Journal. 38 (2007) 1021-1026

[40] Zhang J, Yin Y. SMA-based bionic integration design of self-sensor–actuator-structure for artificial skeletal muscle, Sensors and Actuators A: Physical. 181 (2012) 94-102

[41] Kang S, Lee J, Lee S, Kim S, Kim JK, et al. Maskless Fabrication of Highly Robust, Flexible Transparent Cu Conductor by Random Crack Network Assisted Cu Nanoparticle Patterning and Laser Sintering, Advanced Electronic Materials. 2 (2016) 1600277

[42] Wang Q, Yu P, Bai L, Bao R, Wang N, et al. Self-assembled nano-leaf/vein bionic structure of $TiO_2/MoS_2$ composites for photoelectric sensors, Nanoscale. 9 (2017) 18194-18201

[43] MQ Jian, KL Xia, Q Wang, Z Yin, HM Wang, CY Wang, JH Xie, MC Zhang, YY Zhang. Flexible and Highly Sensitive Pressure Sensors Based on Bionic Hierarchical Structures, Advanced functional materials. 27 (2017) 1606066

[44] M Zou, SC Xu, CG Wei, HX Wang, ZZ Liu. A bionic method for the crashworthiness design of thin-walled structures inspired by bamboo, Thin-Walled Structures. 101 (2016) 222-230

[45] Cai G, Wang J, Lin M-F, Chen J, Cui M, et al. A semitransparent snake-like tactile and olfactory bionic sensor with reversibly stretchable properties, NPG Asia Materials. 9 (2017) e437

[46] Roy P, Ota JR, Srivastava SK. Crystalline ZnS thin films by chemical bath deposition method and its characterization, Thin Solid Films. 515 (2006) 1912-1917

[47] Salim S, Eid M, Salem A, Abou El‐khair H. Nanocrystalline ZnS thin films by chemical bath deposition method and its characterization, Surface and Interface Analysis. 44 (2012) 1214-8

[48] Cheng J, Fan D, Wang H, Liu B, Zhang Y, Yan H. Chemical bath deposition of crystalline ZnS thin films, Semiconductor science and technology. 18 (2003) 676

[49] Chen Z-G, Zou J, Liu G, Lu HF, Li F, et al. Silicon-induced oriented ZnS nanobelts for hydrogen sensitivity, Nanotechnology. 19 (2008) 055710

[50] XF Pana, XJ Zhao, JQ Chena, A Bermaka, ZY Fan, Electrocatalytic property of poly-chromotrope 2B modified glassy carbon electrode on dopamine and its application, Sensors and Actuators B: Chemical. 206 (2015) 764–771

[51] Raj VB, Singh H, Nimal A, Sharma M, Tomar M, Gupta V. Distinct detection of liquor ammonia by ZnO/SAW sensor: Study of complete sensing mechanism, Sensors and Actuators B: Chemical. 238 (2017) 83-90

[52] Raj VB, Singh H, Nimal A, Tomar M, Sharma M, Gupta V. Effect of metal oxide sensing layers on the distinct detection of ammonia using surface acoustic wave (SAW) sensors, Sensors and Actuators B: Chemical. 187 (2013) 563-573

**Declaration of interests**

☒ The authors declare that they have no known competing financial interests or personal relationships that could have appeared to influence the work reported in this paper.

☐ The authors declare the following financial interests/personal relationships which may be considered as potential competing interests:

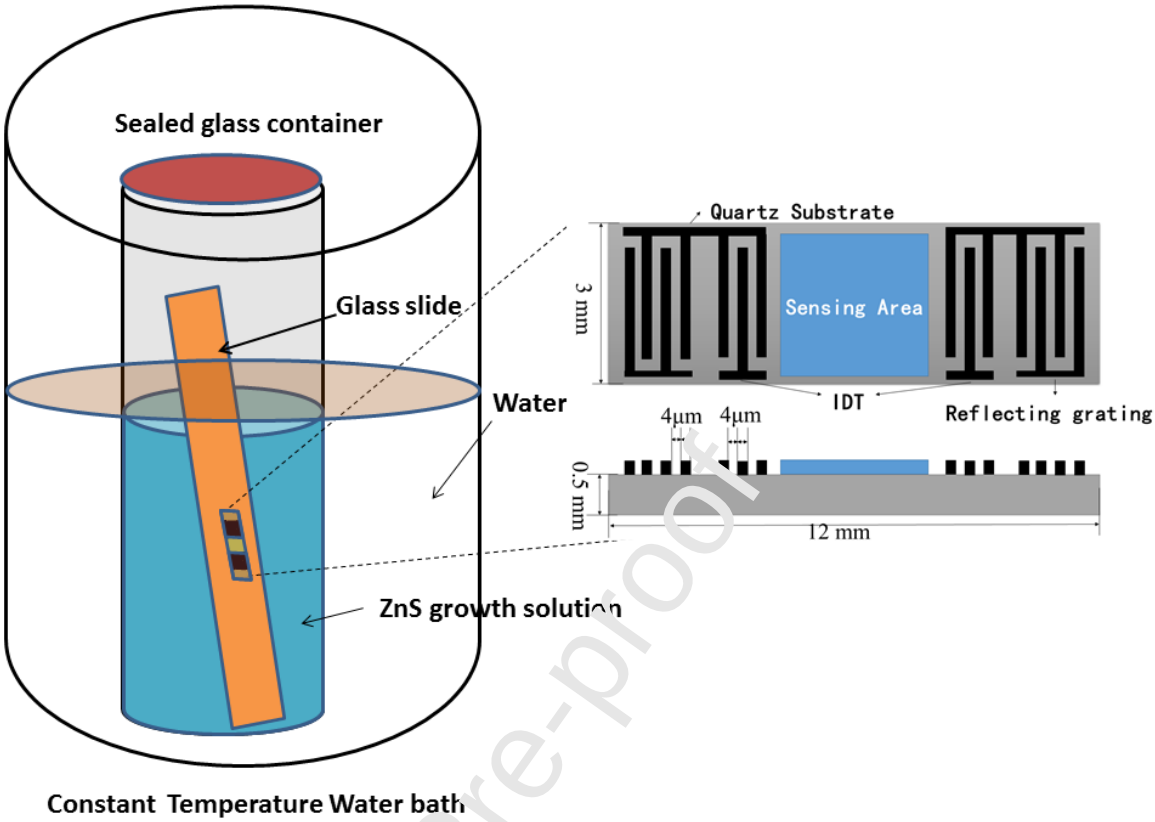


Fig.1 An illustration of preparation of ZnS sensing layer on the SAW device.

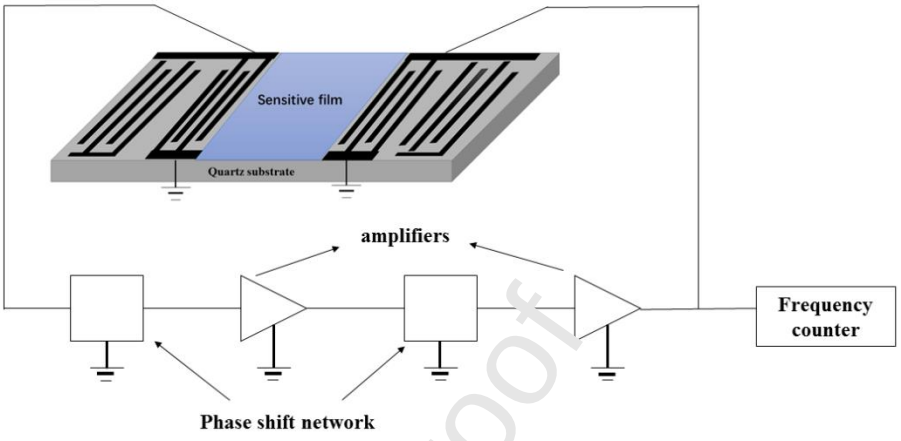


**(a)**

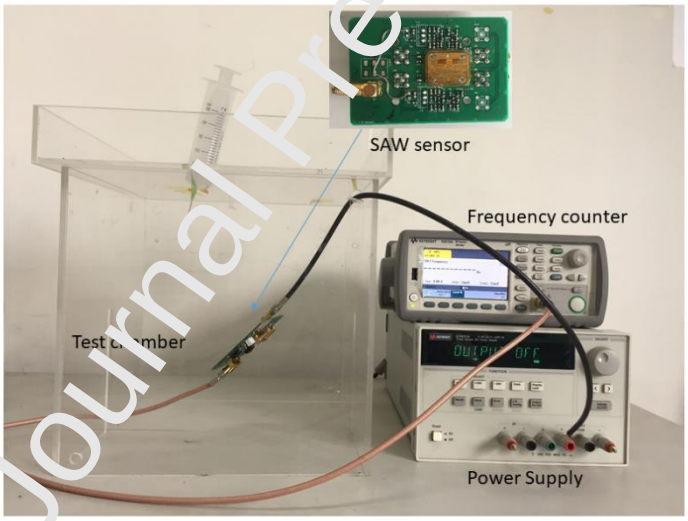


**(b)**

Figure 2. (a) A structural illustration of SAW sensor and its electronic components, and (b) Experimental set-up of SAW gas sensing system.

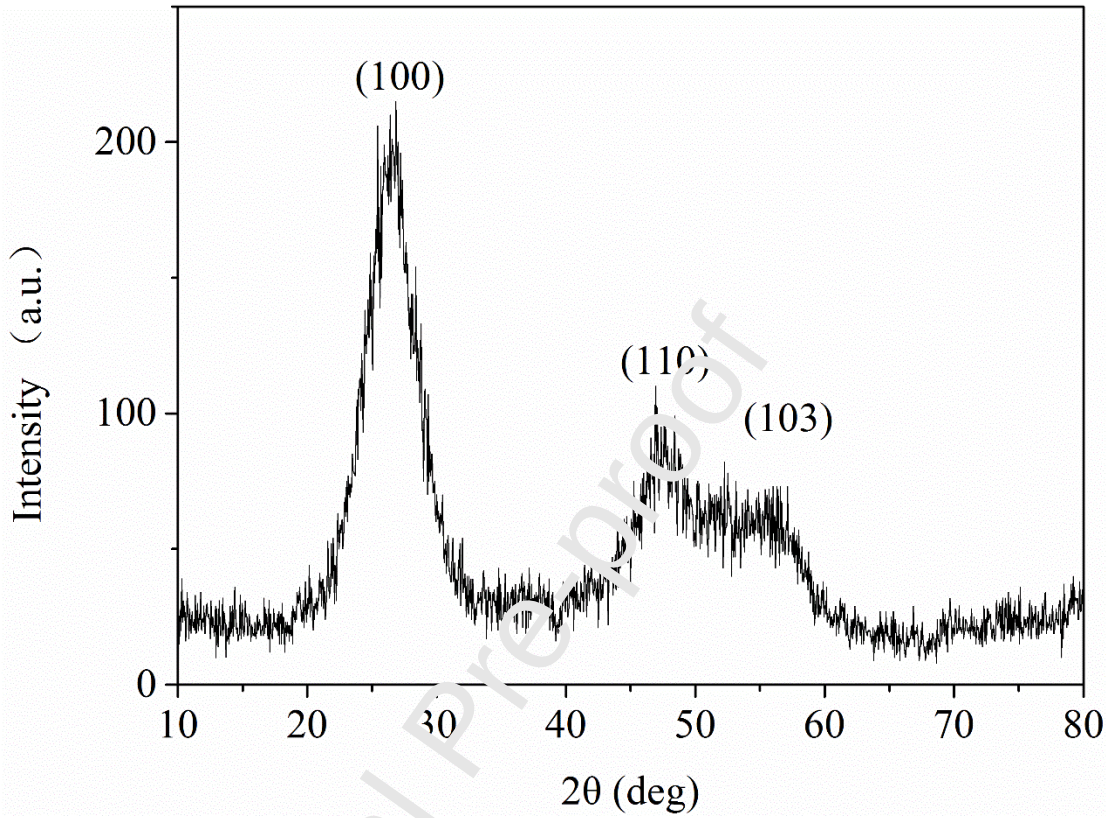


Figure 3. XRD patterns of ZnS nanostructure of sample 4 (deposition for 30 minutes).

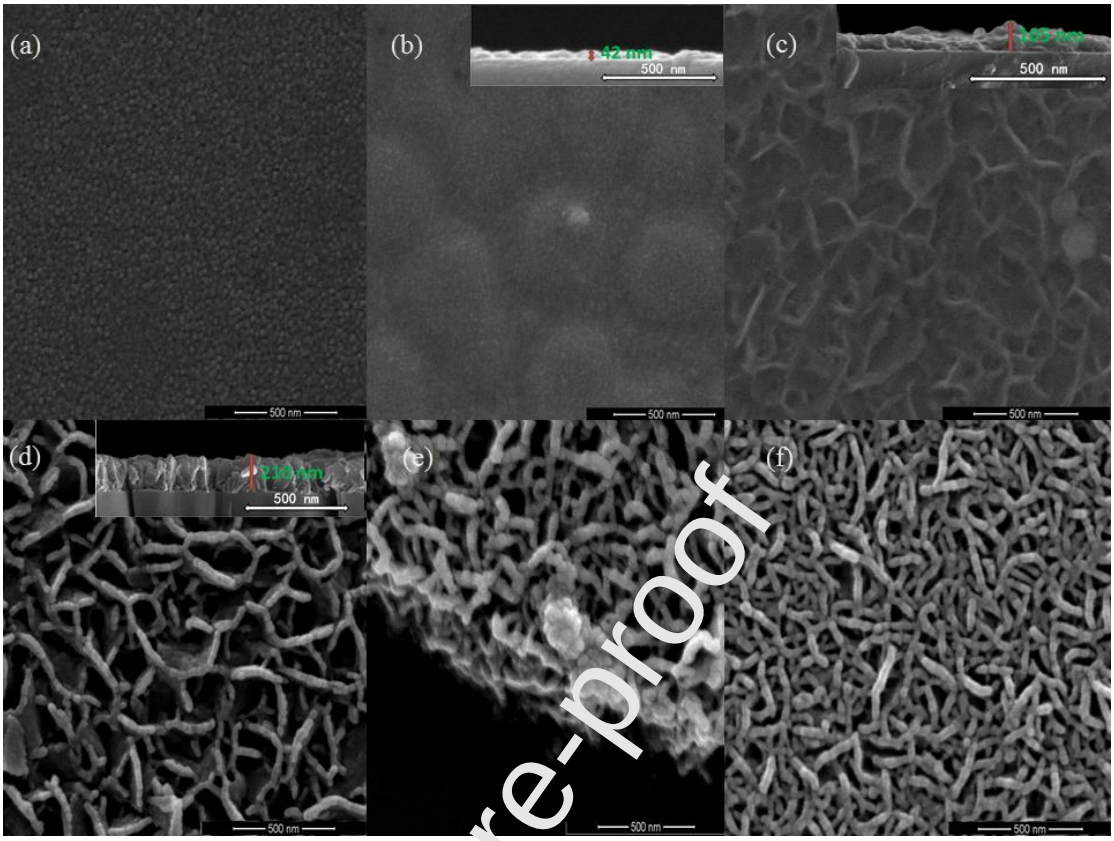


Figure 4. Top-view and cross-section SEM images of ZnS nanostructure for the different film samples. (a) sample 1 (5 min deposition); (b) sample 2 (10 min deposition); (c) sample 3 (20 min deposition); (d) sample 4 (30 min deposition); (e) sample 5 (35 min deposition); and (f) sample 6 (40 min deposition).

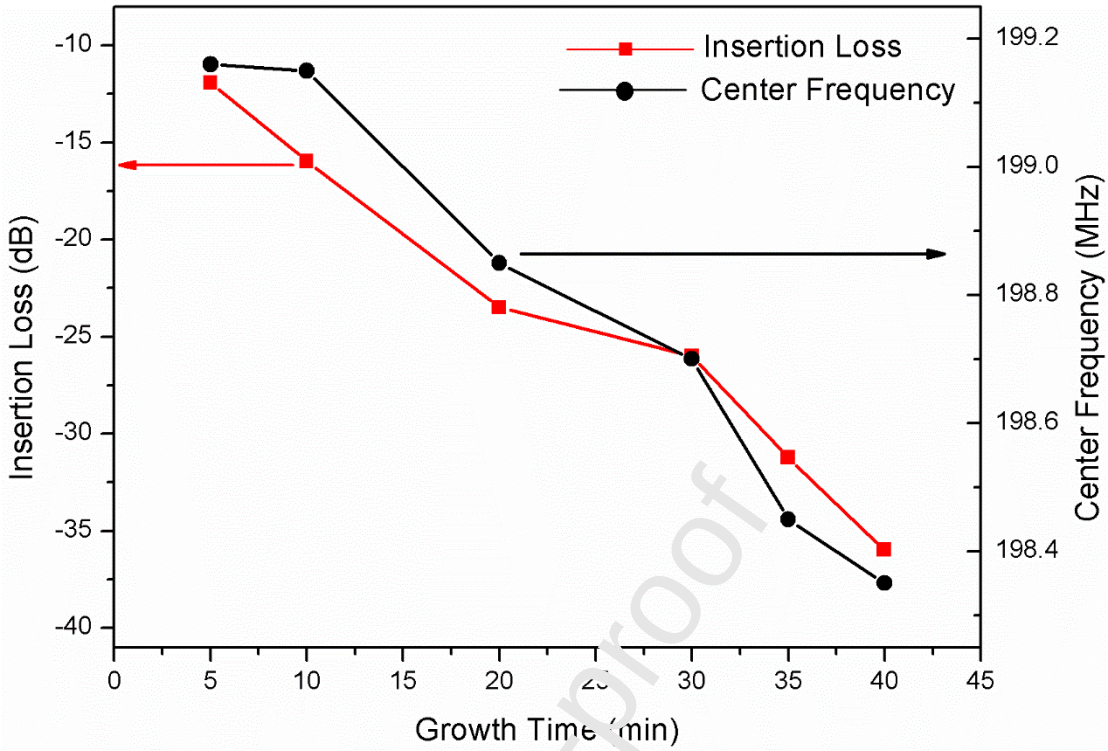


Figure 5. Insertion losses and center frequencies of SAW resonators with different ZnS nanostructured sensing layers.

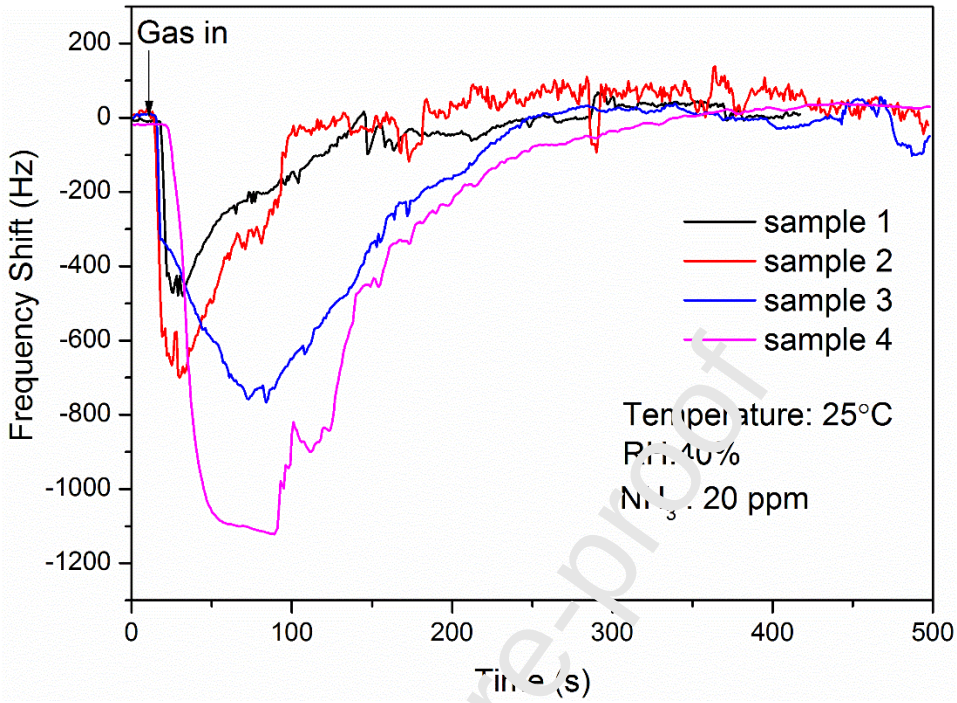


**(a)**

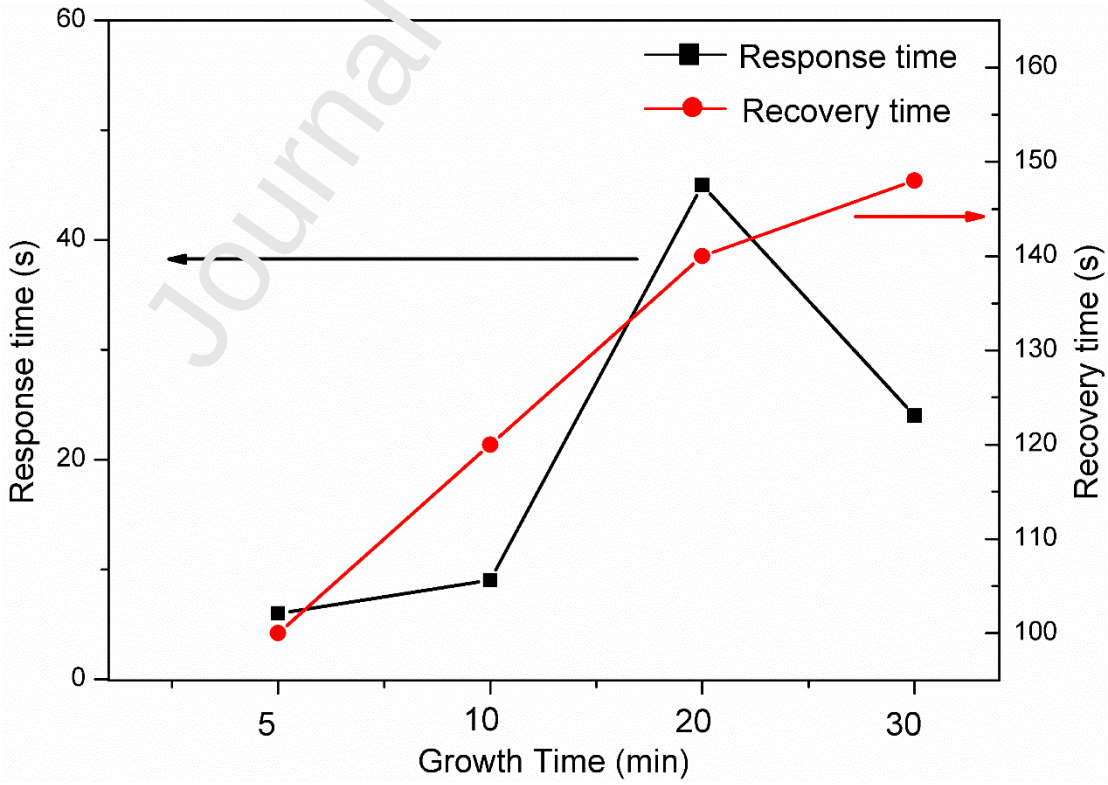

**(b)**

Figure 6. (a) Dynamic responses, and (b) response and recovery times of SAW sensors with different ZnS nanostructures, when exposed to 20 ppm Ammonia.

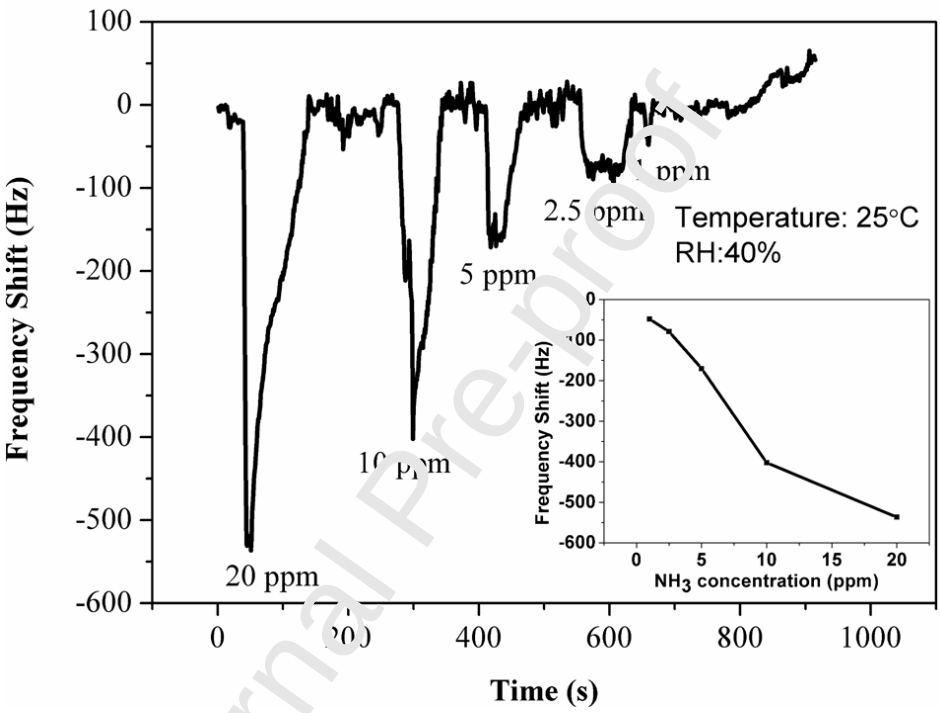


**(a)**

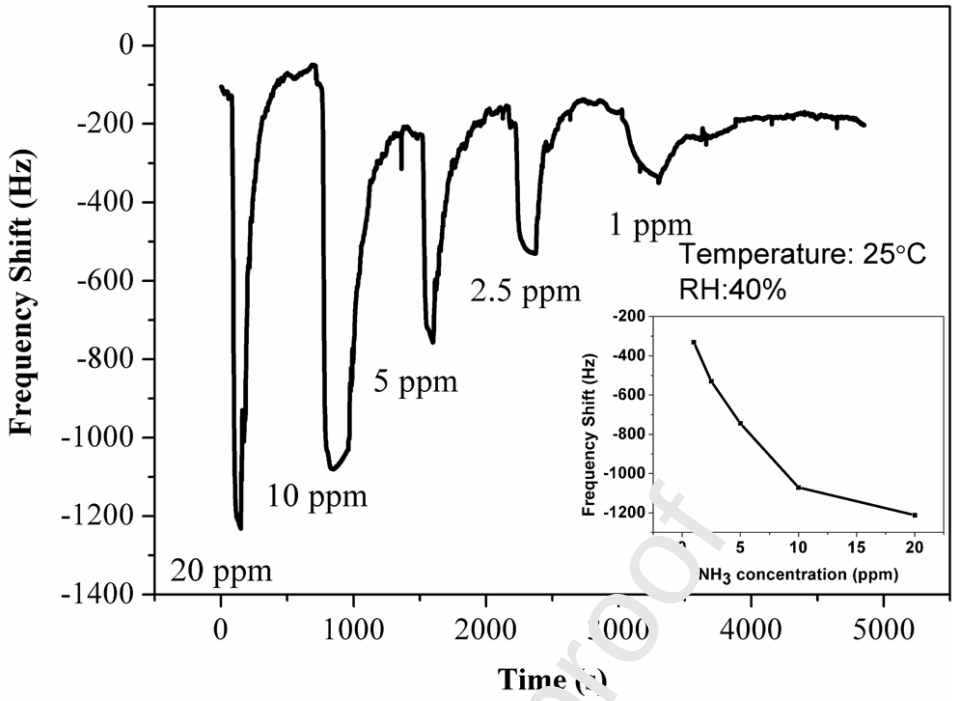


**(b)**

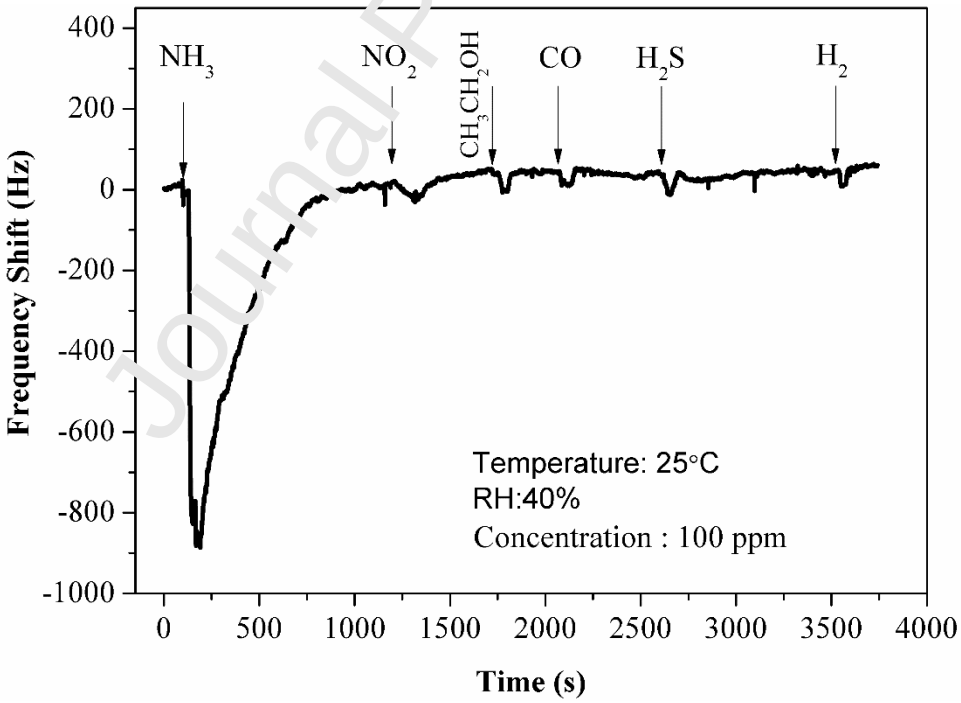


**(c)**

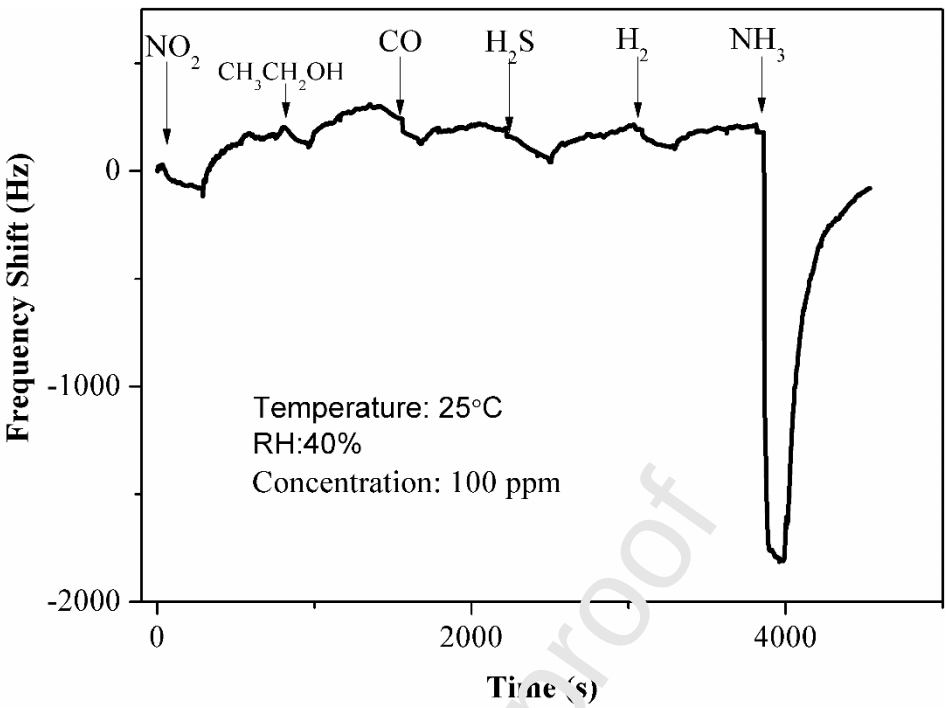


**(d)**

Figure 7. Dynamic responses of SAW sensors to different concentrations of $NH_3$ gas: (a) sample 1 (5 min deposition), and (b) sample 4 (30 min deposition); and to 100 ppm different gases: (c) sample 1 (5 min deposition), and (d) sample 4 (30 min deposition).

# Graphical Abstract

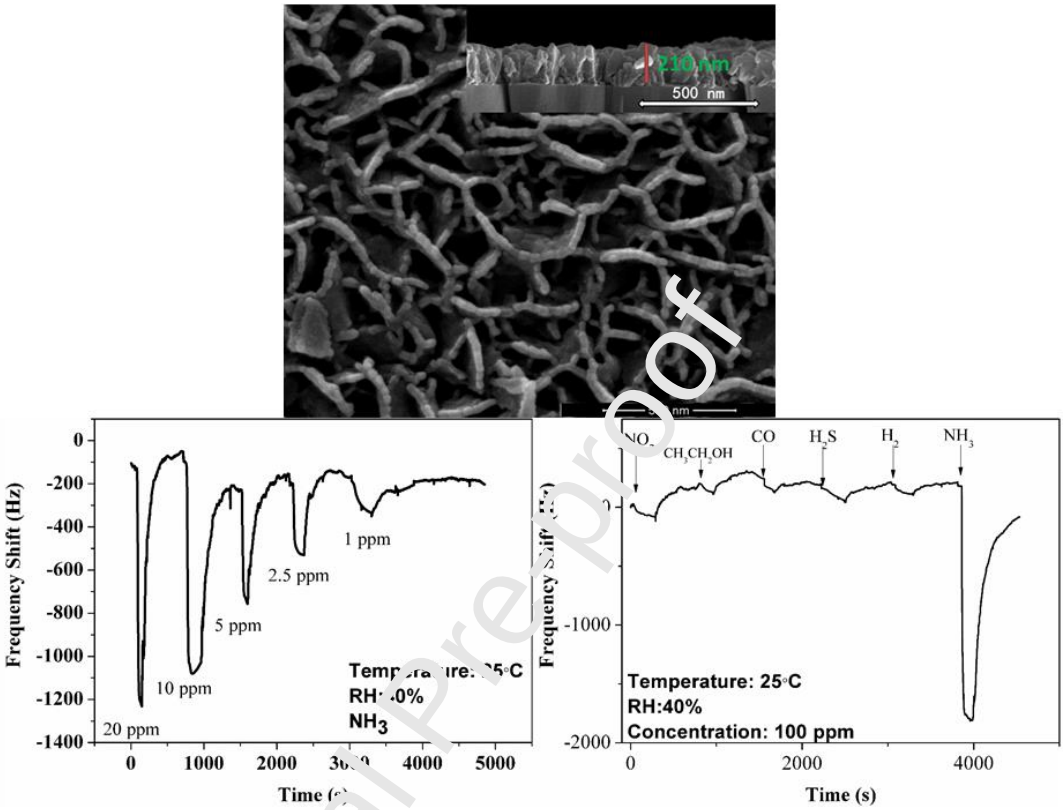

**Highlights**

- Mucosal-like ZnS nanostructures were synthesized using a chemical bath deposition method on surface of ST-cut quartz surface acoustic wave (SAW) device for ammonia sensing applications.
- The SAW device with ZnS mucosal nanostructures achieved a good sensitivity and selectivity to ammonia.
- The negative frequency shift of SAW sensor is associated to the effects of mass loading and electrical loading.